Journal of Asian Earth Sciences 35 (2009) 273–284

Contents lists available at ScienceDirect

Journal of Asian Earth Sciences

journal homepage: www.elsevier.com/locate/jaes

Metamorphic evolution, mineral chemistry and thermobarometry of orthogneiss hosting ultrahigh-pressure eclogites in the North Qaidam metamorphic belt, Western China

C.A. Menold [a,b,*], C.E. Manning [b], A. Yin [b], P. Tropper [c], X.-H. Chen [d], X.-F. Wang [d]

[a] Department of Geology, Albion College, 611 E. Porter St., Albion, MI 49224, USA
[b] Department of Earth and Space Science, University of California, Los Angeles, CA 90095, USA
[c] Geo- and Atmospheric Sciences, University of Innsbruck, Innsbruck, Austria
[d] Institute of Geomechanics, Chinese Academy of Geology Sciences, Beijing, China

ARTICLE INFO

Article history:
Received 12 May 2008
Received in revised form 20 December 2008
Accepted 24 December 2008

Keywords:
UHP
North Tibet
Orthogneiss
Pseudosection
Eclogite
North Qaidam

ABSTRACT

Many UHP terranes contain abundant felsic gneiss with volumetrically minor mafic and ultramafic blocks. The mafic rocks typically preserve the high-pressure assemblages, whereas felsic gneisses preserve low pressure mineral assemblages. In the absence coesite it can be difficult to confirm that felsic lithologies experienced high-pressure conditions. This has lead to uncertainty over the regional extent of UHP terranes. We conducted a detailed study of textures, mineral parageneses and compositions of a suite of eclogite-bearing orthogneisses in the Luliang Shan from the North Qaidam UHP metamorphic belt. Two distinctive gneisses were observed: volumetrically dominant, uniform leucocratic orthogneiss and mica-rich gneiss which occurs only in proximity to eclogite blocks. Two pseudosections have been constructed to constrain the *P–T* conditions recorded by the mineral assemblages and mineral zoning observed in the orthogneiss. Relic high-pressure inclusions and predicted conditions of garnet growth suggest that the orthogneiss followed a metamorphic *P–T* path comparable to the eclogite it encloses, with peak pressure at ~26 kbar very close to the quartz–coesite phase boundary.

1. Introduction

Ultrahigh-pressure (UHP) rocks are found in most continent–continent convergent plate boundaries. The UHP facies field is defined as being above the quartz–coesite phase transition ($P > 26$ kbar) (Coleman and Wang, 1995). Most UHP terranes consist of volumetrically minor mafic and ultramafic lenses, blocks and boudins hosted by gneiss (e.g. Coleman and Wang, 1995; Ernst and Liou, 1995; Harley and Carswell, 1995). The mafic (±ultramafic) rocks typically preserve the highest-pressure assemblages, whereas the host gneisses commonly contain little or no high-pressure mineral indicators. This led to a debate about whether the felsic lithologies experienced the same UHP metamorphic conditions as the mafic and ultramafic rocks they host or whether the latter lithologies were tectonically emplaced after UHP metamorphism (e.g. Harley and Carswell, 1995). Discovery of coesite in zircon from amphibolite facies gneiss that preserved no other indicators of high-pressure in several UHP terranes has contributed to the current consensus that host gneiss and eclogite generally comprise a single, coherent block of continental crust that has been subducted to mantle depths (Ye et al., 2000; Tabata et al., 1998). Determining which rocks in these terranes have a shared *P–T* history can be difficult and is the subject of this study.

The lack of high-pressure indicators in the orthogneiss can be partially explained by the facility of recrystallization in felsic versus mafic rocks. The felsic lithologies contain a higher proportion of hydrous phases and are rheologically weaker than their mafic counterparts. Preservation of high-pressure assemblages in this lithology requires fluid-poor conditions and slow reaction rates during exhumation (e.g. Proyer, 2003). Reports of high-pressure minerals preserved in leucocratic orthogneiss from UHP terranes are scarce and mostly from the Western Alps (Lenze and Stöckhart, 2007; Rowley et al., 1997; Biino and Compagnoni, 1992; Chopin et al., 1991; Le Goff and Bellevre, 1990; Massonne and Chopin, 1989; Oberhänsli et al., 1985) and China (Liu et al., 2006; Carswell et al., 2000; Wallis et al., 1997). High-pressure mineral indicators are jadeite, kyanite, high-silica muscovite (phengite) and coesite. Where high-pressure assemblages are present in felsic rocks it is typically difficult to determine the pressure–temperature (*P–T*) conditions at which they formed (Carswell et al., 2000; Massonne and Chopin, 1989). In particular, high- and medium-pressure geobarometers are generally lacking or of limited use for metagranites

* Corresponding author. Address: Department of Geology, Albion College, 611 E. Porter St., Albion, MI 49224, USA.
E-mail address: cmenold@albion.edu (C.A. Menold).

1367-9120/$ - see front matter © 2009 Elsevier Ltd. All rights reserved.
doi:10.1016/j.jseaes.2008.12.008

(Le Goff and Bellevre, 1990; Proyer, 2003). The approach we apply here involves the calculation of *P–T* pseudosections for specific bulk compositions which can help to fill in the gaps in the *P–T* history of this lithology (Proyer, 2003).

In the North Qaidam metamorphic belt, the first confirmed coesite in the terrane came from a retrograded paragneiss in Dulan (Fig. 1; Yang et al., 2001a); no other ultrahigh-pressure mineral indicators have been reported in crustal rocks of the North Qaidam UHP terrane. Independent pressure–temperature calculations on mafic lithologies yield peak pressure estimates >25 kbar, near the coesite stability field (Yang et al., 2000; Song et al., 2003a,b; Zhang et al., 2004; Zhang et al., 2005a,b,c; Menold et al., submitted for publication). To investigate whether the host orthogneiss shared the same *P–T* history as the mafic eclogites we conducted a detailed study of paragenetic relations, textures and phase equilibria. The result of this investigation is that the gneiss possess previously unrecognized petrologic indicators of early, high-pressure equilibrium, and that their *P–T* path is likely the same as the eclogites they host.

2. Geologic background

The early Paleozoic North Qaidam metamorphic belt is located on the northeastern margin of the Tibetan plateau in northwest China, along the northern margin of the Qaidam Basin (Fig. 1a). Within the metamorphic belt are para-, orthogneisses and marble containing lenses, blocks and boudins of eclogite and garnet peridotite exposed discontinuously from west to east in three localities: Luliang Shan, Xitie Shan and Dulan (Fig. 1b; Mattinson et al., 2007; Zhang et al., 2005a,b,c; Song et al., 2003a,b, 2006; Yang et al., 2002, 2001a). This belt has been inferred to be offset for ~450 km by the Cenozoic left-slip Altyn Tagh fault, with the Altun metamorphic belt (consisting of Jianggelesayi and Bashiwake localities) west of the fault as its offset counterpart (Fig. 1b; Mattinson et al., 2007; Zhang et al., 2001, 2005b,c; Yang et al., 2001a; Yin and Harrison, 2000). When offset is restored the Altun and North Qaidam localities form a ~500 km long northwest trending belt, herein referred to as the North Qaidam UHP/HP metamorphic belt.

Coesite has been reported and confirmed as inclusions in paragneissic zircon from the Dulan locality confirming that the host gneiss experienced UHP metamorphic conditions (Song et al., 2003a,b, 2006; Yang et al., 2002; Yang et al., 2001a,b). Thermobarometric studies throughout the North Qaidam metamorphic belt have yielded peak pressure estimates at or just below the quartz–coesite phase boundary, but peak temperatures vary considerably (Zhang et al., 2001, 2002, 2005a; Song et al., 2003a; Menold et al., submitted for publication). Additional petrologic evidence consistent with UHP metamorphic conditions in the mafic eclogite includes exsolution textures in omphacite and K-feldspar-quartz inclusions (Song et al., 2003a; Mattinson et al., 2007; Zhang et al., 2002). Garnet peridotite in the metamorphic belt also contain evidence of UHP metamorphic conditions, including diamond inclusions in zircon, occurrence of magnesite in lherzolite, and exsolution textures in garnet and olivine (Song et al., 2005a,b, 2004).

The focus of this study is the largest and best exposed locality, the Luliang Shan, a HP–UHP unit made up of abundant quartzo-

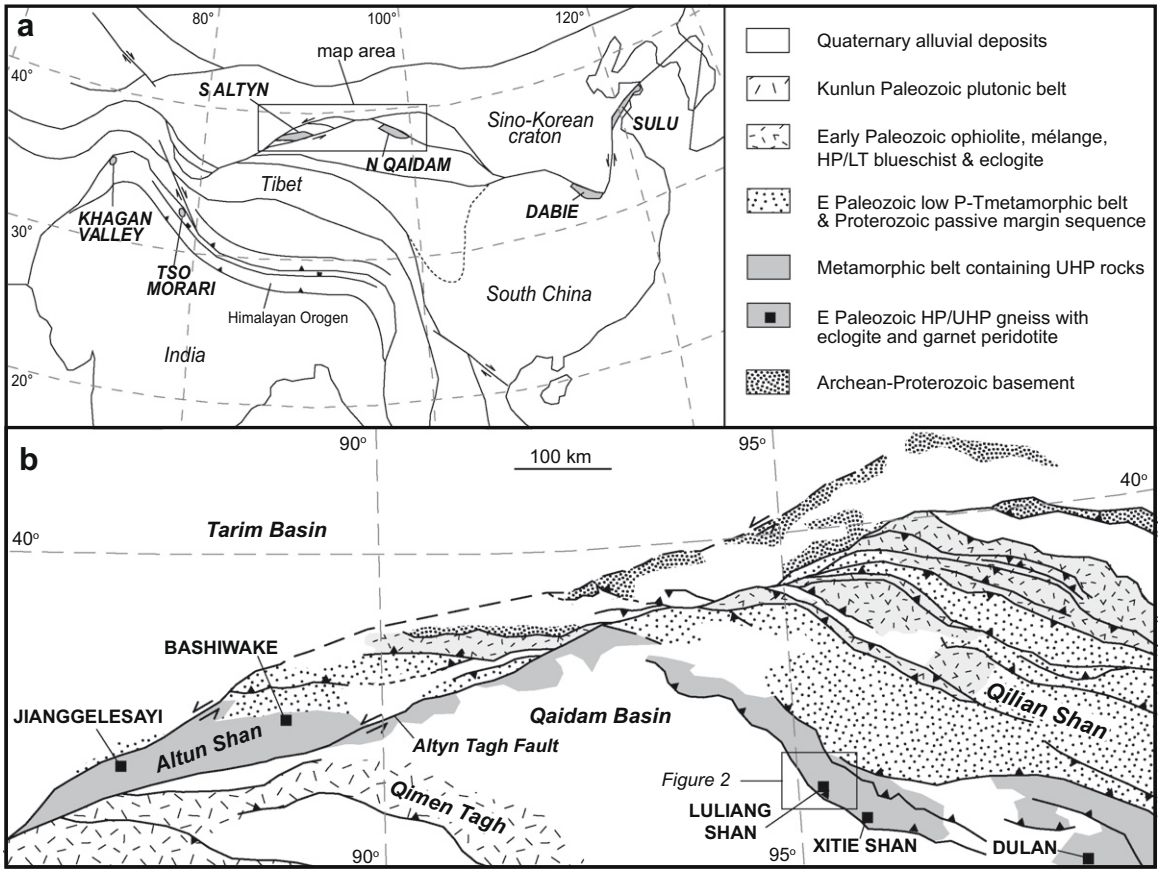

Fig. 1. (a) Simplified terrane map of Asia with UHP localities showing the location of this study (box). Solid lines represent trends of major faults and sutures. (b) Schematic map of North Tibet showing major tectonic units, localities containing eclogite and garnet peridotite, the distribution of lithologic ages and Cenozoic faults (modified from Yin et al. (2002), Gehrels et al. (2003) and Liu (1988)). The box indicates the location of Fig. 2.

feldspathic orthogneiss (gn_{UHP}) with rare paragneiss and marble containing minor mafic eclogite and rare garnet peridotite (Fig. 2). The eclogite and peridotite in the orthogneiss occur as blocks, boudins or layers that are meters to hundreds of meters in size (Fig. 3 a). Cenozoic uplift due to Indo-Asian continental collision has resulted in range-bounding thrusts which have caused high-angle northeast tilting (~70°) of the North Qaidam crust allowing the observation of metamorphic grade and deformational styles over a range of 10 km of crustal thickness (Fig. 2; Jolivet et al. 2001; Yin et al., 2002). This coupled with desert climate conditions has resulted in excellent exposure of the eclogite-bearing orthogneiss unit (Fig. 3a). Pre-Devonian strata in the region are deformed by isoclinal folding and the original bedding has been completely transposed by later development of cleavage and gneissic foliation. A pervasive epidote–amphibolite facies deformation event imparted a common foliation on all units including the eclogite-bearing gneiss. The fabric orientation in the foliated amphibolite rims of eclogite blocks is sub-parallel to the regional epidote–amphibolite facies foliation fabric found in the surrounding orthogneiss and throughout the North Qaidam metamorphic belt. This deformation overprints and post-dates the eclogite-facies assemblage in the mafic eclogite blocks.

A detailed study of the paragenesis and petrology of mafic eclogite from the Luliangshan in the North Qaidam metamorphic belt (Menold et al., submitted for publication) identified four stages of mineral growth: phengite–eclogite facies mineral assemblage in Stage I, early amphibole-eclogite facies assemblage in Stage II; amphibole–eclogite facies assemblage in Stage III, and epidote–amphibolite facies assemblage in Stage IV. No evidence of pre-eclogite facies assemblages were was observed. Stage I records pressures of 25 ± 2 kbar associated with a temperature of 590 ± 25 °C. Stage II minerals record growth during decompression from 24 to 18 kbar, associated with an increase in temperature from 590 ± 25 °C to 650 ± 25 °C. Stage III minerals record continuing decompression and decreasing temperature to 16 ± 2 kbar and 605 ± 25 °C. Stage IV minerals record temperatures of 415–510 °C, with maximum pressure constrained by the epidote–amphibolite facies boundary (~8–9 kbar). The identification of Stage II, III and IV assemblages allows construction of a more detailed clockwise retrograde *P–T* path, revealing that the Luliangshan eclogites experienced heating during the early stages of exhumation (Fig. 4). The temperature estimate at peak pressure (590 °C) is significantly lower than those estimated at other North Qaidam eclogite localities which range from 650 °C to 780 °C suggesting that geothermal gradients varied significantly along strike in the UHP metamorphic belt, both at the maximum depth of lithospheric subduction and at the middle crustal depths to which the eclogite-bearing lithologies resided over 10s of m.y. after UHP metamorphism (Menold et al., submitted for publication).

3. Sample description and petrography

Penetrative deformation during regional metamorphism has converted the felsic protolith to well-foliated gneiss containing the major phases: K-feldspar, albite, white mica, and quartz. Minor phases observed are epidote, apatite, zircon, tourmaline, titanite, rutile, garnet, kyanite and allanite (Fig. 3). Petrographic and field observations indicate that the gneiss does not contain a uniform abundance of phases throughout the unit (Table 1). The largest volume of gneiss (>95%) is uniform in color and mineral assemblage

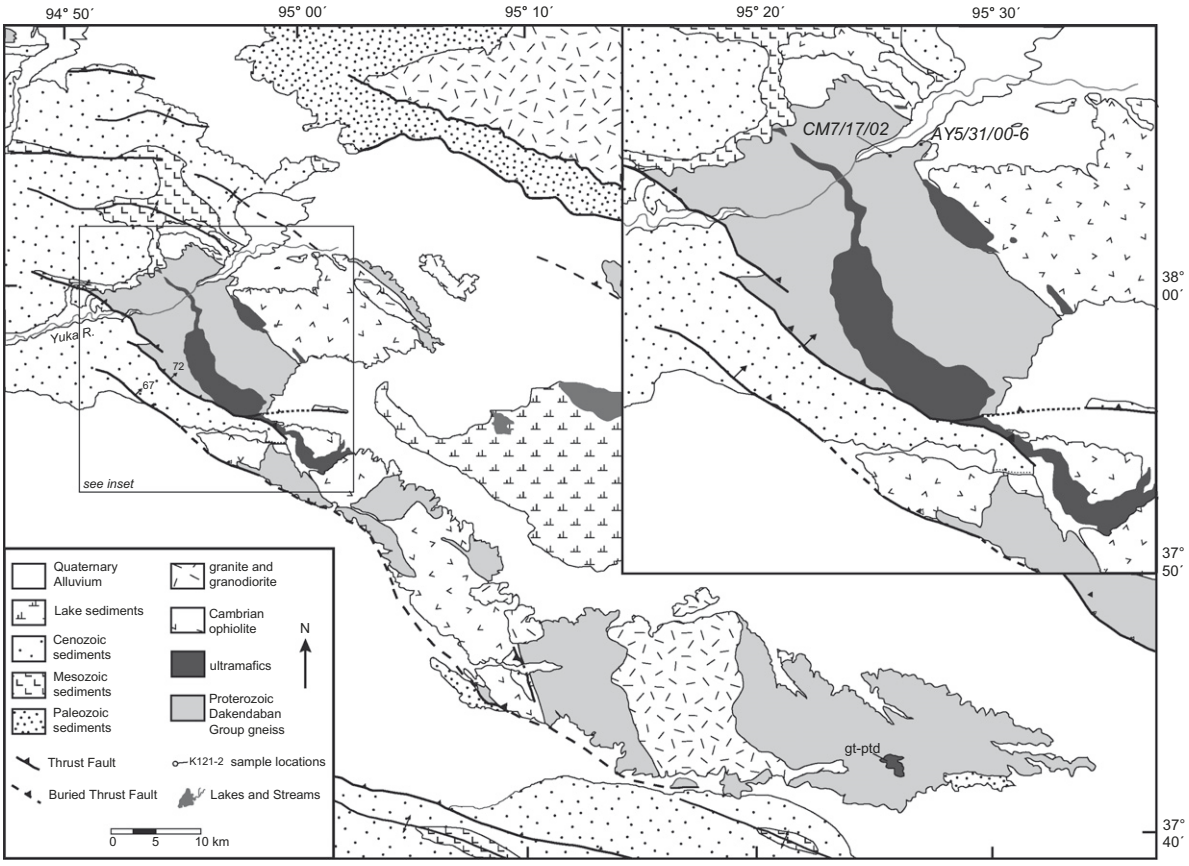

Fig. 2. Simplified geologic map of the Luliang Shan area showing sample locations, the distribution of lithologic units and major Cenozoic faults. Inset box contains eclogite sample localities. Map compiled from our own observations and Qinghai Bureau of Geology and Mineral Resources (1991).

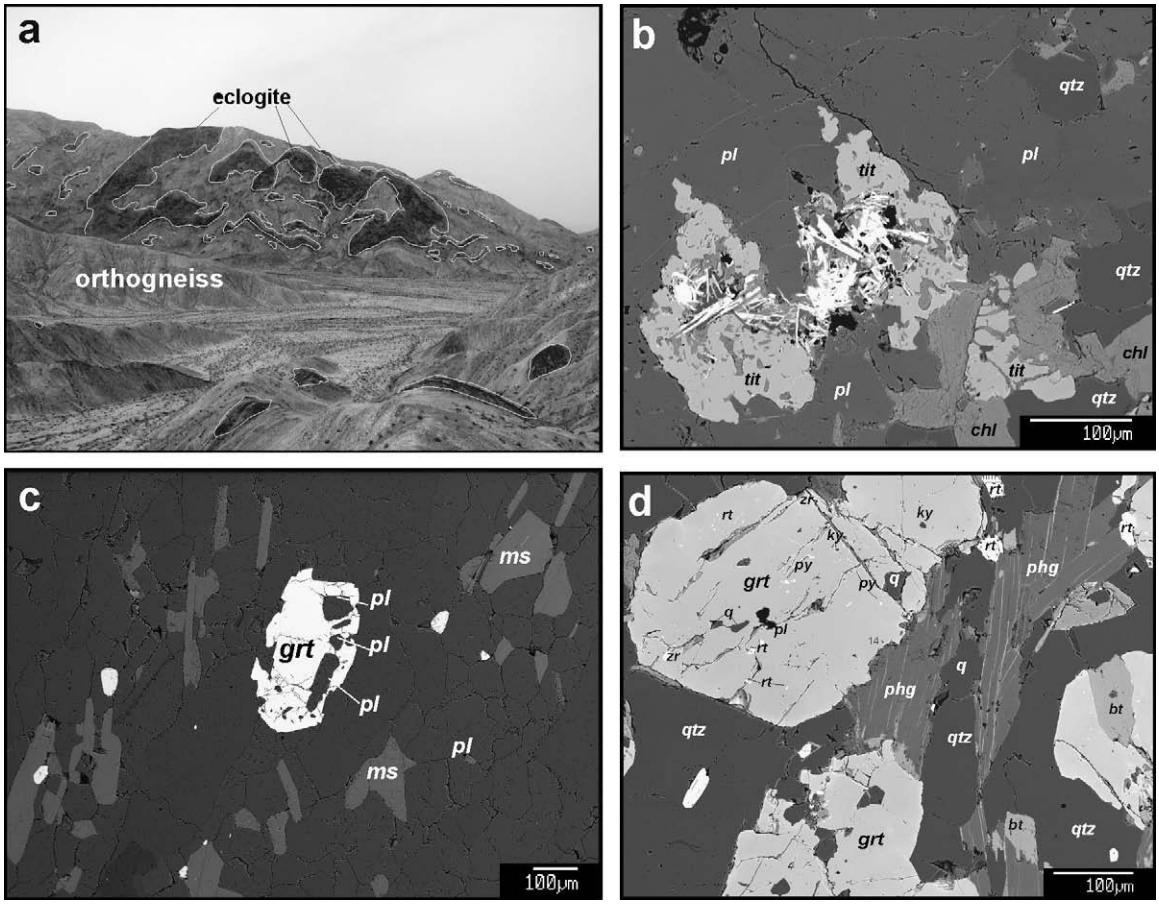

Fig. 3. (a) Photo of UHP orthogneiss unit with numerous boudinaged mafic eclogites. (b) BSE image of a garnet from orthogneiss. (c) BSE image of a garnet from mica-rich gneiss. (d) BSE image of titanite from orthogneiss. Mineral abbreviations after Kretz (1983) except phengite – phg and titanite – tit.

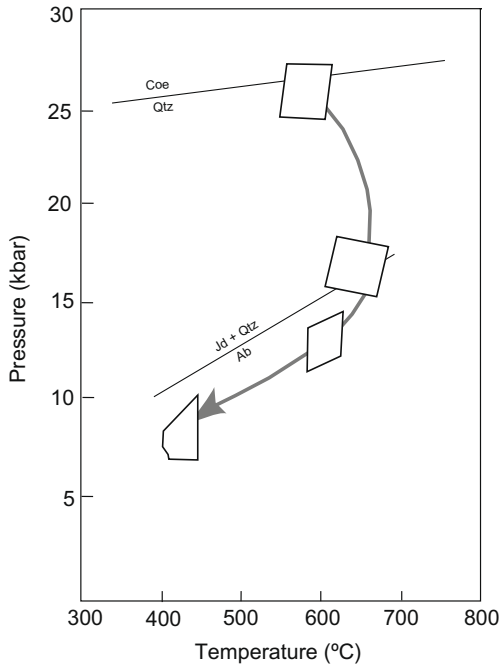

Fig. 4. Pressure–temperature path results for Luliang Shan eclogite (Menold et al., submitted for publication). Mineral abbreviations according to Kretz (1983) except Coe = coesite. Thin lines are curves of the following reactions: jadeite + quartz = albite (Holland, 1980) and coesite = quartz (Mirwald and Massonne, 1980).

(Table 1; CM 7/17/02-1, -3, -4). The mineral assemblage consists of white mica, plagioclase, K-feldspar, and quartz with minor paragonite, tourmaline, epidote, titanite/ilmenite and apatite ± garnet. Samples typically have abundant white mica predominantly muscovite often intergrown with paragonite (~30% total volume) which defines the foliation observed throughout the unit (Table 3; Fig. 3). Feldspar is also abundant, up to 60% of the total assemblage, occurring as plagioclase and K-feldspar. Garnets are rare and small (<600 μm), often inclusion-free but when present the inclusion population consists of albite, quartz and white mica (Fig. 3c and d). Rare matrix titanite is also present (Fig. 3b). This gneiss is here forward called an orthogneiss.

Within 5 m of the mafic eclogite blocks the gneiss contains >40% white mica, here forward called the mica-rich gneiss. The mineral assemblage consists of white mica, quartz, plagioclase, garnet and ilmenite with minor paragonite, epidote and apatite (±kyanite, allanite, rutile, titanite). The mica-rich gneiss contains textural evidence of multiple generations of white mica, not observed in the orthogneiss (Table 1; Fig. 3d). It is typified by large, coarse white micas grains (1–2 mm), usually partially overgrown and cross cut with sub-parallel finer-grained white mica, biotite and/or chlorite. The earlier coarse white mica occurs with abundant quartz and plagioclase. Large, metamict allanite grains are rimmed by epidote. Rare anhedral titanite grains occur as a matrix phase in one granodioritic gneiss sample (CM7/17/02-6) and anhedral rutile grains occur as a matrix phase in another (CM 7/17/02-8; Fig. 3d). Garnets are typically ~500 μm in diameter and contain numerous small inclusions (Fig. 3d). Garnet rims contain rutile, quartz and plagioclase inclusions; garnet cores contain inclusions

Table 1
Modal abundances of minerals in gneiss samples (determined by point counting).

Sample ID	Distance (m)	% Qtz	% Phg	% Ms	% Pg	% Kfs	% Pl	% Grt	% Rt	% Tit	% Ilm	% Ap	% Bt	% Chl	% Ep	% Tur	% Oxides	Ave g.s. (mm)
CM 7/17/02-1	23	45	0	10	0	0	40	3	tr	0	0	1	0	0	0	1	tr	0.4
CM 7/17/02-2	17	10	0	30	0	25	30	1.5	0	0	0	1	0	tr	0	2	3	0.9
CM 7/17/02-3	12	55	0	20	0	0	20	5	0	0	0	0	0	tr	0	0	tr	0.8
CM 7/17/02-4	5	25	5	55	0	0	0	3	tr	0	8	0	5	0	tr	0	tr	0.25
CM 7/17/02-5	3	35	0	40	10	0	1	6	0	0	0	0.5	8	tr	0	0	hem	1
CM 7/17/02-6	2.5	23	17	5	0	0	7	0	0	5	5	0	1	30	1	0	hem	0.2
CM 7/17/02-7	2	42	1	32	15	0	1	1	0	0	0	tr	0	0	tr	0	7	0.4
CM 7/17/02-8	1.5	35	10	20	0	0	0	17	2	0	4	1	10	1	0	0	tr	0.25
CM 7/17/02-9	1	30	0	27	5	2	3	2	0	0	0	tr	0	10	0	0	7	0.2
CM 7/17/02-10	0.5	36	0	29	16	0	9	3	0	0	0	tr	1	0	0	2	tr	0.35
CM 7/17/02-11	0.25	34	0	24	12	0	25	0	0	0	0	1	0	0	0	0	tr	0.15
CM 7/17/02-12	0.05	35	30	2	0	tr	5	5	tr	0	0	0	9	3	0	0	0	0.3

Note: Mineral abbreviations according to Kretz (1983) except Phg = phengite and Tit = titanite. Other abbreviations: ave. g.s.= average grain size, tr = trace.

of rutile, kyanite, phengite, quartz and zircon (Fig. 3d). No jadeite inclusions have been observed. No petrographic evidence has yet been found to indicate that coesite was previously stable in these rocks.

The lowest grade assemblage observed in the eclogite-bearing gneiss unit (gn_{UHP}) is a greenschist facies assemblage containing chlorite, biotite, quartz and hematite. In mica-rich gneiss samples, chlorite and biotite replace garnet and the coarse white mica. This type of replacement alteration is most pronounced in mica-rich gneiss samples near contacts with eclogite. Tiny (<1 μm) hematite needles occur in between cleavage planes of the coarse white mica possibly because it is phengite which contains significantly more Fe and Mg than end-member muscovite (Fig. 3d).

4. Whole-rock geochemistry

Whole-rock bulk chemical analyses were performed on 13 gneiss samples taken from the northeastern part of the eclogite-bearing gneiss unit (gn_{UHP}) in the Luliangshan (Fig. 2); the samples were taken at a variable distances from eclogite blocks and consisted of both quartz-rich orthogneiss samples and mica-rich gneiss samples. The rocks were crushed using a mortar and pestle to <3 mm and powdered in a tungsten-carbide shatterbox at UCLA. Whole-rock abundances of major and minor elements were determined by a lithium metaborate/tetraborate fusion ICP and the trace elements by ICP/MS at Actlabs in Ancaster, Ontario, Canada. The whole-rock major element data is summarized in Table 2 with significant figures reflecting analytical uncertainty.

The two gneiss types have distinct bulk compositions: (1) the orthogneiss samples that occur throughout the unit and in all samples taken from more than 5 m away from contacts with mafic eclogite have silica-rich compositions (SiO_2 > 75 wt%) and (2) the mica-rich gneiss samples found only within 5 m of eclogite blocks have intermediate compositions (SiO_2 = 60–66 wt%; Fig. 5a; Table 2). The orthogneiss contains more sodium (2–5%) than potassium (1–3%), high values of normative albite (40–65%) and plots in and near the trondjemite field of Barker (1979); the mica-rich gneiss is enriched in potassium (3–4%) with low sodium (0–1%), much less normative albite (5–10%) and plots in the granite field (Fig. 5b; Table 3). In general, the mica-rich gneiss is enriched in Fe, Mg, Ca and K, and depleted in Si and Na (Fig. 5a; Table 2). The proximity of mica-rich gneiss to eclogite contacts suggests that there has been locally significant major element transport between the eclogite adjacent gneiss during its metamorphic history.

5. Mineral composition

Mineral compositions were determined with a JEOL 8200 electron microprobe at University of California, Los Angeles, with five wavelength dispersive spectrometers. Operating conditions were 15 nA beam current, and 15 keV accelerating potential. Raw counts were collected for 15 s and converted to oxide wt% by the ZAF correction procedure and natural and synthetic mineral standards. Minerals were analyzed with a focused (<1 μm) beam, except for plagioclase and micas, for which a 5 and 10 μm spot were used respectively to limit volatilization. Representative mineral compositions are listed in Tables 4 and 5. Special attention was paid to the determination of the full compositional range of garnet and phengite, both within and between grains.

5.1. Garnet

The orthogneiss and mica-rich gneiss have distinct garnet morphology, composition and zoning (Figs. 3 and 6; Table 4). Garnets from the orthogneiss have sparse inclusions and relatively uniform grossular- and almandine-rich cores ($Alm_{50-60}Grs_{35-50}Sps_{1-12}Prp_{0-4}$)

Table 2
Major element whole-rock geochemistry from gneiss samples, major element values are reported in wt%; ND, not detected.

Sample ID	Description	SiO_2	Al_2O_3	Fe_2O_3	MnO	MgO	CaO	Na_2O	K_2O	TiO_2	P_2O_5	LOI	Total
AY 5/31/00-6c	Orthogneiss	75.44	14.51	1.04	0.00	0.22	0.51	3.69	2.69	0.11	0.12	1.34	99.67
CM 7/17/02-1	Orthogneiss	75.92	14.30	0.95	0.05	0.06	0.48	4.76	2.01	0.02	0.22	1.05	99.82
CM 7/17/02-3	Orthogneiss	75.51	14.70	0.99	0.06	0.13	0.67	5.05	1.61	0.03	0.18	0.80	99.71
CM 7/17/02-5	Orthogneiss	78.69	14.34	0.48	ND	0.10	0.35	1.89	1.70	0.01	0.19	1.88	99.63
CM 7/17/02-7	Orthogneiss	81.95	8.10	2.21	0.02	0.76	0.66	1.91	1.08	0.44	0.06	2.67	99.87
CM 7/17/02-9	Orthogneiss	74.68	14.95	1.31	0.01	0.69	0.97	2.63	2.63	0.06	0.21	1.64	99.79
CM 7/17/02-11	Orthogneiss	76.18	14.21	0.82	0.01	0.11	0.74	5.50	0.89	0.02	0.25	1.02	99.75
CM 7/17/02-4	Mica-rich gneiss	62.87	15.97	7.25	0.05	2.99	1.51	0.64	3.93	0.87	0.12	3.70	99.91
CM 7/17/02-6	Mica-rich gneiss	61.97	15.44	8.32	0.07	4.45	1.35	1.19	2.45	0.88	0.11	3.66	99.89
CM 7/17/02-8	Mica-rich gneiss	60.39	16.63	7.66	0.06	3.35	0.81	0.75	4.13	0.86	0.09	4.29	99.00
CM 7/17/02-12	Mica-rich gneiss	65.87	14.78	6.32	0.07	2.54	1.61	0.96	4.10	0.69	0.11	2.88	99.92

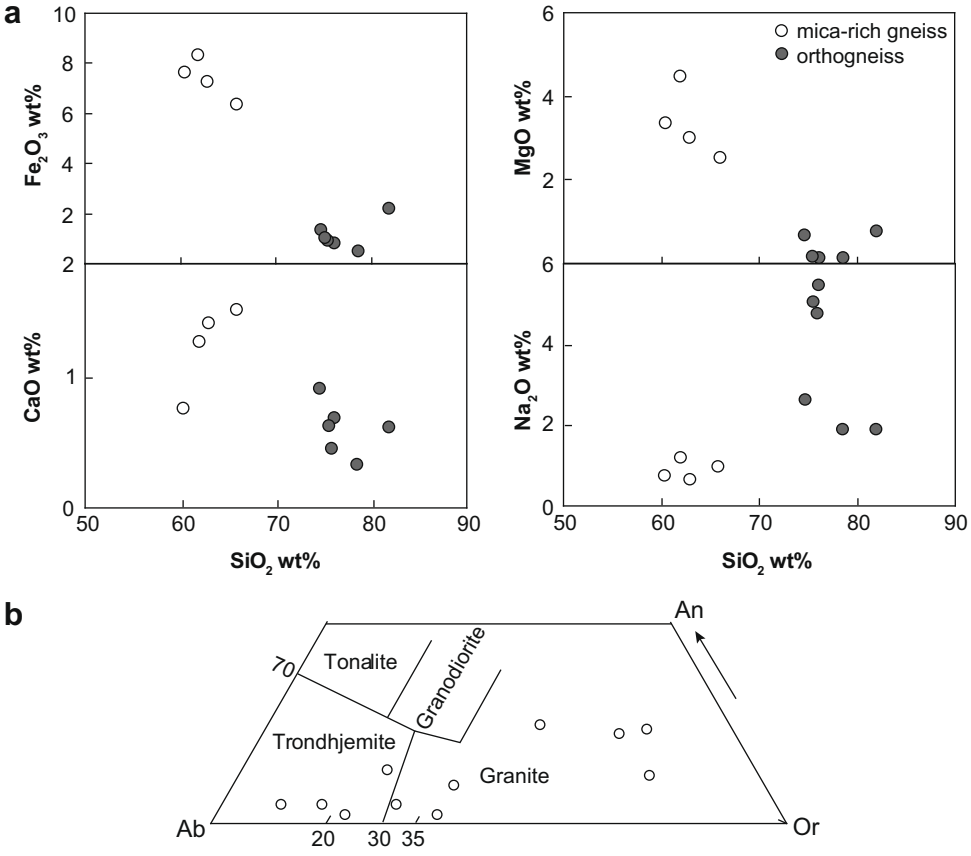

Fig. 5. Whole-rock geochemistry plots of gneiss samples from the Luliang Shan. White, proximal (<5 m); grey, distal (>5 m). (a) The two compositional groups correlate with distance from eclogite blocks. Samples near eclogite blocks are enriched in Fe, Mg and Ca and depleted in Na and Si. (b) Normative feldspar compositions with classification scheme from Barker (1979). An, normative anorthite; Ab, normative albite; Or, normative orthoclase.

surrounded by narrow (<10 μm) almandine-enriched rims ($Alm_{50–70}Grs_{15–25}Sps_{5–15}Prp_{4–7}$) (Fig. 3c and 5a), whereas garnets from the mica-rich gneiss have abundant inclusions and grossular-, spessartine- and almandine-rich cores ($Alm_{30–40}Grs_{20}Sps_{10–45}Prp_{05–10}$) and almandine- and pyrope-rich ($Alm_{50–75}Grs_{0–8}Sps_{1–6}Prp_{12–50}$) rims (Fig. 6a). Maximum modal grossular (X_{Ca}) values in orthogneiss garnet occur in the cores of grains (X_{Ca} = 0.35–55) and show a strong negative correlation with modal almandine/pyrope (Fe/Mg) ratios (Fig. 6b). Maximum X_{Ca} values in garnets from mica-rich gneiss are significantly lower and do not occur in the cores; the cores of these garnets record the lowest X_{Ca} observed (Fig. 6a). The Fe/Mg ratios in the mica-rich gneiss garnet are significantly lower with less variation from core to rim than those observed in the orthogneiss garnet reflecting the higher pyrope component in these garnets (Fig. 6b and c).

5.2. White Mica

White mica occurs throughout gneiss from the eclogite-bearing gneiss unit (gn_{UHP}), but silica content varies widely from 3.0 to 3.4 silicon atoms per formula unit (p.f.u.; Fig. 7; Table 5). The slight deviation from the ideal muscovite–celadonite join observed in these samples may be due to the presence of Fe^{3+} or sub-microscopic biotite. The high-silica mica (>3.12 Si p.f.u.) is termed phengite; the low silica mica (3.12–3.00 Si p.f.u.), muscovite. Phengite with the highest silica content mostly occurs as armored

Table 3
Normative mineral assemblages calculated for gneiss samples (values are reported in modal %; NA, not available).

Sample ID	IUGS classification	Qtz	Crn	Or	Ab	An	Hy	Mt	Ilm	Hem	Ap
AY 5/31/00-6c	Granite	43.8	5.2	14.1	31.2	1.8	0.6	NA	0.02	1.0	0.3
CM 7/17/02-1	Trondjemite	40.1	4.0	12.0	40.2	1.0	0.2	0.1	0.04	0.9	0.5
CM 7/17/02-3	Trondjemite	39.9	3.9	9.5	42.7	2.2	0.3	0.1	0.05	0.9	0.4
CM 7/17/02-5	Granite	60.9	9.2	10.0	16.0	0.5	0.3	NA	NA	0.5	0.4
CM 7/17/02-7	Trondjemite	64.4	2.7	6.4	16.2	2.9	1.9	NA	0.05	2.2	0.1
CM 7/17/02-9	Granite	48.8	6.5	15.5	22.2	3.5	1.7	NA	0.03	1.3	0.5
CM 7/17/02-11	Trondjemite	39.8	3.4	5.3	46.5	2.0	0.3	NA	0.02	0.8	0.6
CM 7/17/02-4	Granite	36.8	8.2	23.2	5.4	6.7	7.4	NA	0.11	7.3	0.3
CM 7/17/02-6	Granite	36.5	8.6	14.5	10.1	6.0	11.0	NA	0.15	8.3	0.2
CM 7/17/02-8	Granite	33.8	9.7	24.4	6.3	3.4	8.3	NA	0.12	7.7	0.2
CM 7/17/02-12	Granite	37.7	6.1	24.2	8.1	7.3	6.3	NA	0.14	6.3	0.2

Note: Normative mineral abbreviations according to Kretz (1983) except Hy, hypersthene.

Table 4
Garnet composition from orthogneiss and mica-rich gneiss. Garnet formulae were normalized to 12 oxygen atoms and Fe^{2+}/Fe^{3+} ratios were estimated by the charge-balance recalculation technique of Droop (1987).

Sample	6c	6c	6c	6c	1	1	4	4	4	8	8
Position	Core	Core	Rim	Rim	Core	Rim	Core	Core	Rim	Core	Rim
Type	ogn	ogn	ogn	ogn	ogn	ogn	m-gn	m-gn	m-gn	m-gn	m-gn
SiO_2	37.74	38.21	37.83	37.87	37.00	36.97	39.09	38.80	39.11	38.53	38.68
MgO	0.08	0.15	0.14	0.22	0.15	0.14	6.15	5.56	5.91	8.85	7.25
Na_2O	0.02	0.02	0.00	0.00	0.07	0.06	0.00	0.03	0.07	0.02	0.01
Al_2O_3	21.39	21.62	21.38	21.54	21.13	21.08	21.86	21.74	21.74	22.22	22.44
FeO	19.42	20.29	25.38	24.47	24.47	24.42	26.70	26.54	27.28	26.85	24.44
MnO	2.88	3.43	1.61	1.52	4.75	10.09	0.33	0.32	0.36	0.31	0.33
Cr_2O_3	0.00	0.01	0.00	0.03	0.00	0.00	0.00	0.00	0.07	0.00	0.00
K_2O	0.00	0.04	0.03	0.02	0.00	0.00	0.02	0.00	0.00	0.00	0.00
CaO	18.08	17.61	14.61	14.82	12.29	7.58	5.70	6.21	5.78	2.78	7.15
TiO_2	0.04	0.10	0.03	0.01	0.09	0.00	0.03	0.06	0.08	0.03	0.00
Total	99.65	101.49	101.00	100.51	99.95	100.31	99.88	99.25	100.40	99.92	100.30
Si	2.98	2.97	2.98	2.99	2.96	2.98	3.03	3.03	3.03	2.96	2.97
Al	1.99	1.98	1.99	2.01	1.99	2.00	2.00	2.00	1.98	2.01	2.03
Ti	0.00	0.01	0.00	0.00	0.01	0.00	0.00	0.00	0.00	0.00	0.00
Fe^{3+}	0.04	0.05	0.05	0.01	0.09	0.04	0.00	0.00	0.00	0.05	0.04
Cr	0.00	0.00	0.00	0.00	0.00	0.00	0.00	0.00	0.00	0.00	0.00
Mg	0.01	0.02	0.02	0.03	0.02	0.02	0.71	0.65	0.68	1.02	0.83
Fe^{2+}	1.25	1.27	1.63	1.61	1.55	1.60	1.73	1.73	1.77	1.65	1.53
Mn	0.19	0.23	0.11	0.10	0.32	0.69	0.02	0.02	0.02	0.02	0.02
Ca	1.53	1.47	1.23	1.26	1.05	0.65	0.47	0.52	0.48	0.23	0.59
Na	0.00	0.00	0.00	0.00	0.01	0.01	0.00	0.00	0.01	0.00	0.00
Fe^{2+}/Mg	129	75	97	61	91	95	2.4	2.7	2.6	1.6	1.8
X_{Mg}	0.00	0.01	0.01	0.01	0.01	0.01	0.24	0.22	0.23	0.36	0.28
X_{Fe}	0.45	0.46	0.57	0.56	0.59	0.71	0.59	0.59	0.60	0.57	0.52
X_{Ca}	0.55	0.53	0.42	0.42	0.40	0.29	0.16	0.18	0.16	0.09	0.21

Note: Modal chemical abundances (X) renormalized without Mn to facilitate comparison to pseudosections. 6c, AY5/31/00-6c; 1, 4 and 8, CM7/17/02-X; ogn, orthogneiss; m-gn, mica-rich gneiss.

Table 5
Phengite compositions from orthogneiss and mica-rich gneiss from electron microprobe analyses. Mica formulae were calculated by normalizing to 11 oxygen atoms and all Fe was assumed to be ferrous.

Sample	6c	6c	6c	1	1	4	4	4	8	8
Position	Matrix	Matrix	Matrix	Matrix	Matrix	In gt	Matrix, c	Matrix, r	Matrix	Matrix
Type	ogn	ogn	ogn	ogn	ogn	m-gn	m-gn	m-gn	m-gn	m-gn
SiO_2	47.78	47.43	46.44	46.51	46.00	50.41	46.90	46.20	49.52	48.39
MgO	0.62	0.53	0.65	0.32	0.21	3.21	1.71	1.34	3.14	2.70
Na_2O	0.26	0.08	0.11	0.43	0.56	0.70	0.48	0.56	0.72	0.75
Al_2O_3	31.45	33.13	33.58	33.96	34.56	28.01	30.59	31.61	29.20	30.29
FeO	3.23	4.39	3.72	2.63	2.01	1.57	1.64	1.41	1.49	1.56
MnO	0.01	0.06	0.05	0.00	0.03	0.02	0.00	0.00	0.00	0.00
Cr_2O_3	0.06	0.02	0.04	0.00	0.00	0.07	0.00	0.00	0.00	0.00
K_2O	11.25	10.22	10.58	10.86	10.84	9.70	10.84	10.35	9.49	9.89
CaO	0.04	0.06	0.02	0.02	0.02	0.00	0.02	0.06	0.01	0.00
TiO_2	0.46	0.13	0.29	0.04	0.04	0.42	0.40	0.08	0.34	0.39
Total	95.16	96.04	95.48	94.39	94.27	94.10	92.58	91.62	93.99	93.98
Si	3.22	3.17	3.12	3.14	3.11	3.38	3.23	3.20	3.32	3.26
Al	2.50	2.59	2.66	2.70	2.71	2.21	2.48	2.58	2.17	2.41
Ti	0.02	0.01	0.01	0.00	0.00	0.02	0.02	0.00	0.01	0.02
Cr	0.00	0.00	0.00	0.00	0.00	0.00	0.00	0.00	0.00	0.00
Mg	0.06	0.05	0.06	0.03	0.02	0.32	0.18	0.14	0.32	0.27
Fe	0.18	0.25	0.21	0.15	0.12	0.09	0.09	0.08	0.09	0.09
Mn	0.00	0.00	0.00	0.00	0.00	0.00	0.00	0.00	0.00	0.00
Ca	0.00	0.00	0.00	0.00	0.00	0.00	0.00	0.00	0.00	0.00
Na	0.03	0.01	0.01	0.06	0.08	0.09	0.06	0.08	0.09	0.10
K	0.97	0.87	0.91	0.94	0.93	0.83	0.95	0.92	0.81	0.85
Total	7.00	6.96	7.00	7.01	7.02	6.95	7.02	7.00	6.96	6.99
Fe/Mg	2.92	4.7	3.2	4.6	7.2	0.28	0.50	0.57	0.79	0.72

Note: 6c, AY5/31/00-6c; 1, 4 and 8, CM7/17/02-X; ogn, orthogneiss; m-gn, mica-rich gneiss; c, core; r, rim.

inclusions in garnet (>3.3 Si p.f.u.) and in the matrix of mica-rich gneiss samples near to eclogite blocks. White mica grains forming the matrix schistosities typically have Si < 3.3 p.f.u. (Fig. 7). The phengites also show a strong negative correlation of Fe^{total}/Mg with Si content (Fig 7b).

5.3. Titanite and Rutile

Rare titanite grains occur in the matrix of one sample from each type of gneiss (AY5/31/00-9b, CM7/17/02-9). The titanite contains significant aluminum substitution (0.11–0.22 p.f.u.). There is a

strong negative linear correlation between Ti and $Al + Fe^{3+}$ and a positive correlation between F and $Al + Fe^{3+}$ indicating a coupled substitution: $Ti^{4+} + O^{2-} = (Al, Fe^{3+}) + (F, OH)^{-}$ (e.g. Enami et al. 1993). Tiny (<10 μm) rutile grains are preserved in the matrix and as armored inclusions within garnets from the mica-rich gneiss.

5.4. Other minerals

K-feldspar (Or_{96-100}) and albite (Ab_{91-99}) are abundant in the orthogneiss. Albitic plagioclase (Ab_{70-85}) is sparsely observed in the mica-rich gneiss and significantly more calcium-rich than orthogneiss albite. Epidote, when present, is zoned as progressively more pistacite-rich overgrowths (Ps_{23-83}) around allanite grains. Blue tourmaline, zircon, allanite, and apatite occur as minor phases. Chlorite and biotite are present in mica-rich gneiss replacing white mica and garnet.

6. *P–T* history of orthogneiss

Thermobarometric studies of orthogneiss from UHP terranes are rare because metagranites rarely preserve any relic high-pressure phases making traditional thermobarometry difficult. Fe^{2+}–Mg partitioning between garnet and phengite can be used to calculate temperature (Green and Hellman, 1982; Massonne and Chopin, 1989).

Garnets from the orthogneiss are generally inclusion-free but when present the inclusion population consists of albite, quartz and white mica (Fig. 3c), suggesting that garnet grew below the Jadeite + Quartz = Albite equilibrium (Powell, 1985). The strongly negative correlation of Fe/Mg ratio with X_{Ca} in garnet from the orthogneiss suggests cooling during the growth (Fig. 6b). Rim compositions of the garnet have lower Ca contents and much higher Fe/Mg ratios (i.e. lower *T*) suggesting that the last phase of garnet growth was in the amphibolite facies (Fig. 6b; Proyer, 2003; Carswell et al., 2000). The phengite grains in the orthogneiss have Si p.f.u. is 3.22. High Fe^{total}/Mg ratios imply high temperature growth (Fig. 7b). Matrix phengite and garnet from orthogneiss sample AY5/31/00-6c yield temperatures of 600 ± 25 °C (at 18 ± 2 kbar) consistent with eclogite facies thermobarometric calculations (Fig. 4, Tables 4 and 5). However, the very low Mg concentration and unknown Fe^{2+}/Fe^{3+} in the mica indicates caution should be used in evaluating results.

Garnets from the mica-rich gneiss have abundant small inclusions (<10 μm); the cores of these garnets contain inclusions of high-pressure phases, kyanite, phengite and rutile (Fig. 3d). Maximum X_{Ca} values in garnets from mica-rich gneiss are significantly lower than in the orthogneiss garnet and do not occur in the cores; the cores of these garnets record the lowest X_{Ca} observed (Fig. 6c). The Fe/Mg ratios in the mica-rich gneiss garnet are significantly lower with less variation from core to rim than those observed in the orthogneiss garnet reflecting the higher pyrope component in these garnets (Fig. 6b and c). The phengites from the mica-rich gneiss show a strong negative correlation of Fe^{total}/Mg with Si content (Fig. 7b), suggesting that the P_{max} phengites did not form at T_{max} (Carswell et al., 2000). Phengite from mafic eclogites hosted by the orthogneiss also display this compositional feature (Menold et al., submitted for publication) perhaps suggesting that both lithologies experienced a similar *P–T* evolution through comparable peak pressure conditions. Titanites in this study contain evi-

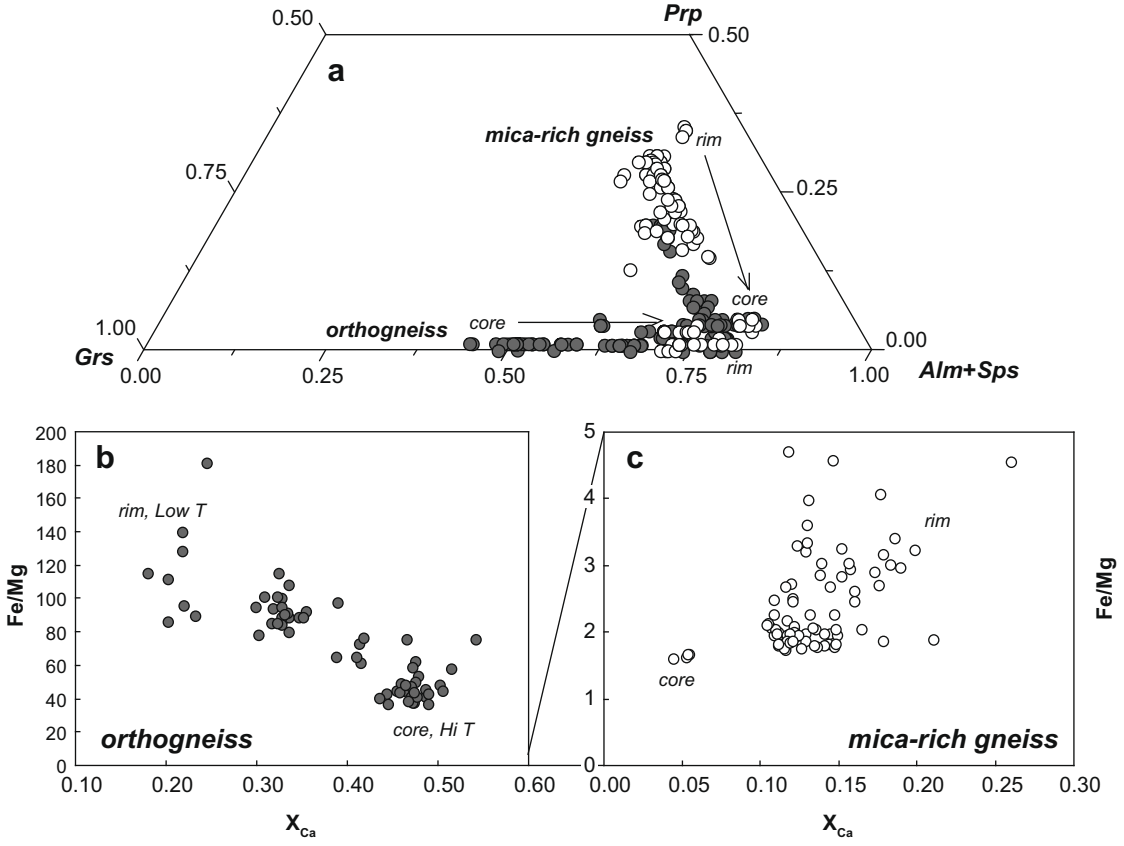

Fig. 6. Garnet compositions from gneiss samples. White, orthogneiss (<5 m), grey, mica-rich gneiss (>5 m). (a) Ternary plot with garnet compositions from gneiss samples, with core and rim compositions designated. Mineral abbreviations from Kretz (1983). (b) Fe/Mg vs. grossular proportion of garnet from orthogneiss vs. the Fe/Mg ratio. (c) Fe/Mg vs. grossular component of garnet from mica-rich gneiss.

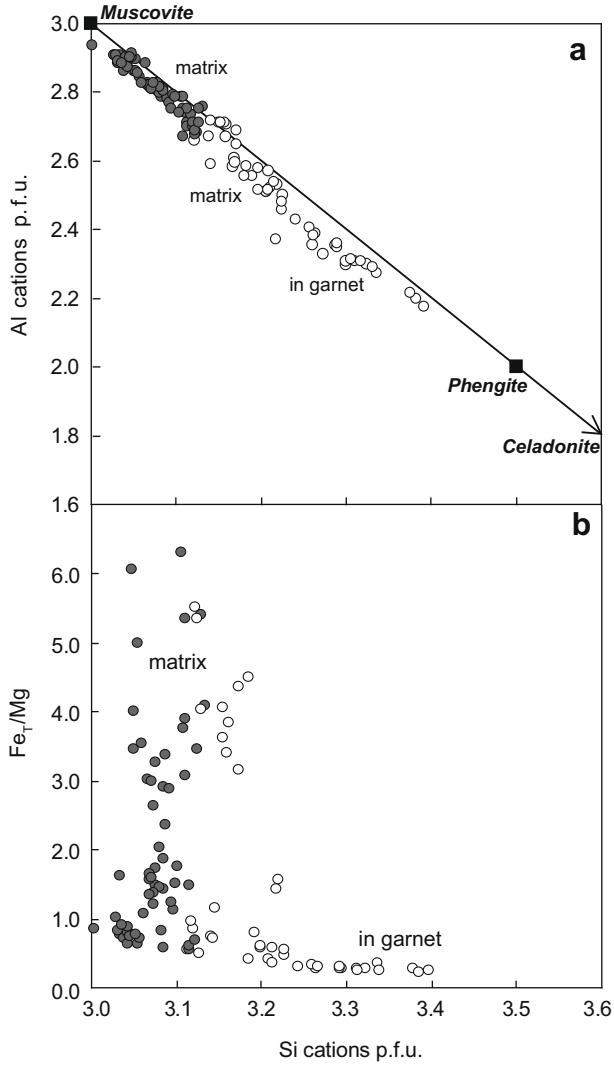

Fig. 7. Phengite compositions in gneiss samples. (a) Al vs. Si cations per formula unit. (b) Fe_{total} vs. Si cations per formula unit.

dence of AlF-substitution which has been suggested to reflect elevated pressure (Troitzsch and Ellis, 2002; Chopin and Ferraris, 2003); titanites from the matrix of a coesite-bearing orthogneiss from Dabie Shan UHP terrane have a similar compositional range (Carswell et al., 2000).

7. *P–T* pseudosections

While somewhat suggestive of high-pressure conditions none of above observations allow for the determination of a constrained pressure–temperature path. To achieve this the eclogite-bearing gneiss paragenesis has been modeled over a range of pressure and temperature by using the thermodynamic database of Holland and Powell (1998) and the program PERPLEX of Connolly (1990) to compute *P–T* pseudosections (e.g., Connolly and Kerrick, 2002). One pseudosection was constructed for each of the two bulk compositional groups observed in the Luliang Shan eclogite-bearing gneiss (AY5/31/00-6c; CM7/17/02-4; Table 2).

A key assumption in the construction of pseudosections, as in any fixed-bulk composition calculation, is that the system is in overall equilibrium. This behavior is at best only approximated in real systems because minerals are commonly zoned and relicts of several different equilibria may be present in the same rock. Furthermore, rocks are often heterogeneous on a fine scale making it difficult to define a representative bulk composition. Despite these difficulties, phase diagram sections constructed for a specified bulk composition, i.e., pseudosections, can be surprisingly useful in thermobarometry because many assemblages have restricted stability fields for specific compositions. Perhaps the most important application of pseudosections in this context is that they offer a practical model for the average behavior of rocks in metamorphic systems, like the gneisses of this study, that resist evaluation using traditional thermobarometric methods (Proyer, 2003).

The following components were used to construct the pseudosections: TiO_2, Al_2O_3, FeO, MgO, MnO, CaO, Na_2O, K_2O, with SiO_2 in excess. Both systems were assumed to be water saturated ($a_{H_2O} = 1$). The assemblages were computed using VERTEX (Connolly, 1990) with end-member data from Holland and Powell (1998) and the following solution models: garnet, non-ideal (Holland and Powell, 1998); phengite (Holland and Powell, 1998); plagioclase (Newton et al., 1980); and epidote, non-ideal (Holland and Powell, 1998).

7.1. Results – orthogneiss

The majority of the Luliang Shan eclogite-bearing gneiss has a silica-rich composition represented by the orthogneiss (Fig. 5). A *P–T* pseudosection has been calculated using a bulk composition typical of this group (AY5/31/00-6c) for the *P–T* window 400–800 °C and 15–30 kbar (Fig. 8a; Table 1). The *P–T* path calculated for the mafic eclogites has been overlain for comparison. Isopleths tracking garnet compositions throughout the *P–T* space have also been calculated for the grossular, almandine and pyrope components (Fig. 8b); prediction of a spessartine component was not supported by the program and the low to moderate concentrations observed in garnets from AY5/31/00-6c make this an acceptable simplification (Table 4).

For this composition and *P–T* window, no pyrope component is predicted in garnet. The cores of garnet from this sample contain $X_{Ca} \sim 50\%$, in the pseudosection there are two places where this composition is predicted; at high pressure (24 kbar at 600 °C) and medium-high pressure (20 kbar at 635 °C; Fig. 8). The inclusion population observed in garnets from the orthogneiss does not contain rutile, jadeite, or phengite but rather albite and quartz indicating that a lower pressure intersection better represents the conditions of growth of the high-Ca garnet. The garnet rims have significantly lower $X_{Ca} \sim 25\%$, predicted during decompression from the medium-high-pressure constraint, not at high pressure (Fig. 8). The garnet composition from core to rim constrains a narrow zone in *P–T* space on the pseudosection; made smaller by the observation that rutile is not the stable Ti-bearing phase in this assemblage (Fig. 8). Three Ti-bearing phases occur in the field of the pseudosection, rutile, titanite and ilmenite; titanite stability was calculated without an Al-solution model. In the rock samples only titanite and ilmenite are observed. The rutile-out reaction is pressure dependent occurring at 17–22 kbar.

7.2. Results – mica-rich gneiss

The mica-rich orthogneiss within 5 m of eclogite blocks has lower bulk silica (Fig. 4, Table 1); a *P–T* pseudosection has been calculated using a bulk composition typical of this group (CM7/17/02-4) for the *P–T* window 400–800 °C and 15–30 kbar (Fig. 9). The *P–T* path calculated for the mafic eclogites has been overlain for comparison. Isopleths tracking garnet compositions throughout the *P–T* space have been calculated for the grossular, almandine and pyrope components (Fig. 9b); prediction of a spessartine component was not supported by the program and the very low concen-

tration observed in garnets from CM7/17/02-4 make this an acceptable simplification (Table 4).

The bulk compositional difference of the mica-rich gneiss results in a significantly different pseudosection topology. Rutile is

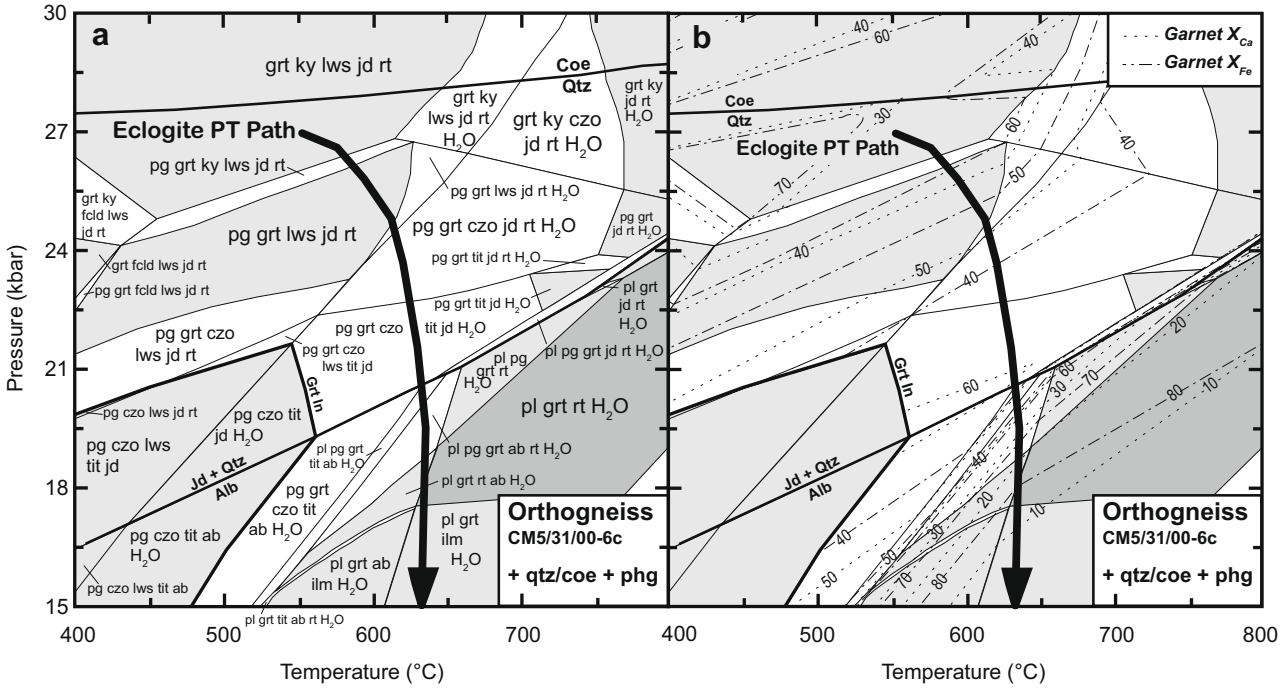

Fig. 8. (a) *P–T* pseudosection phase diagram summarizing the phase relations in the orthogneiss (CM5/31/00-6c). Thin solid lines separate mineral assemblages. Quartz or coesite and phengite are predicted in all assemblages. The thick dark lines denote important reaction boundaries: jadeite + quartz = albite, coesite = quartz and the first appearance of garnet. The thickest black line is the *P–T* path calculated for the mafic eclogite (Fig. 4). Mineral abbreviations according to Kretz (1983) except coe = coesite, phg = phengite and tit = titanite. (b) The same pseudosection with mineral assemblages removed for clarity. Dashed lines are calculated isopleths for Ca and Fe mole fractions in garnet.

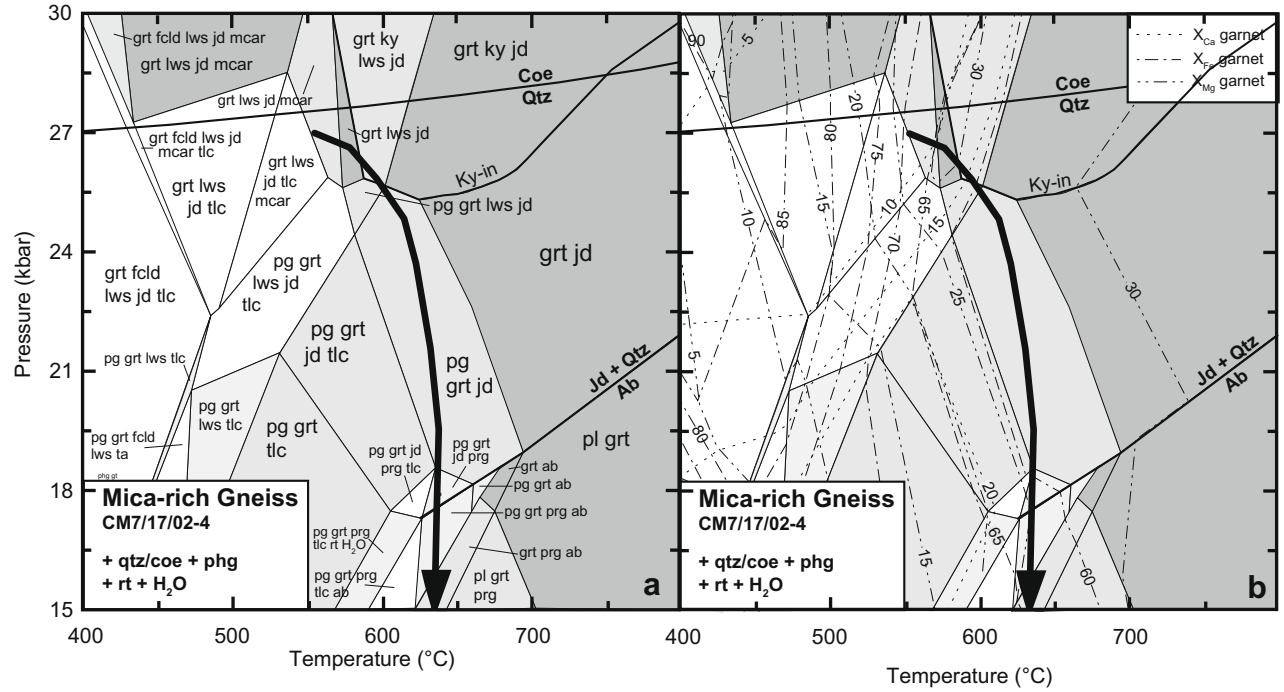

Fig. 9. (a) *P–T* pseudosection phase diagram summarizing the phase relations in the mica-rich gneiss (CM7/17/02-4). Thin solid lines separate different mineral assemblages. Quartz or coesite, phengite and rutile are predicted in all assemblages. The thick dark lines denote important reaction boundaries: jadeite + quartz = albite, coesite = quartz and first appearance of kyanite. The thickest black line is the *P–T* path calculated for the mafic eclogite (Fig. 4). Mineral abbreviations according to Kretz (1983) except coe = coesite and phg = phengite. (b) The same pseudosection with mineral assemblages removed for clarity. Dashed lines are calculated isopleths for Ca, Mg and Fe mole fractions in garnet.

the stable Ti-bearing phase for the entire *P–T* range in the pseudosection consistent with the observation of rutile as a matrix phase and inclusion in garnet in the mica-rich gneiss (Fig. 3d). Garnet is also stable everywhere in the *P–T* range, consistent with the more mafic bulk composition of the mica-rich gneiss; significant pyrope component is predicted (Fig. 9b). Garnet cores in the mica-rich gneiss have a very low grossular content $X_{Ca} < 10\%$ and contain inclusions of kyanite, rutile, phengite (3.4 Si p.f.u.), and quartz. Kyanite is predicted only at pressures greater than 25 kbar (Fig. 9a). The garnet composition ($X_{Ca} < 10\%$) with coexisting inclusion assemblage appear at one point the *P–T* range, at 26 kbar and ~630 °C (Fig. 9), within error of the thermobarometric *P–T* calculation for the peak stage in the mafic eclogites: 570–600 °C, >27 kbar (Fig. 4). This independent evidence suggests that the eclogite and host gneiss experienced similar the peak metamorphic conditions.

The rims of the garnets in the mica-rich gneiss have higher grossular concentrations ($Alm_{50-75}Grs_{0-8}Sps_{1-6}Prp_{12-50}$), with rutile inclusions (no kyanite) and slightly lower Fe/Mg ratios. The pseudosection predicts that they likely formed at lower pressures and higher temperatures than the cores, an observation also made in the mafic eclogites (Fig. 9).

An assumption implicit in the use of the mica-rich gneiss in this study is that the major element exchange with the mafic lithology occurred prior to UHP metamorphism. The high-pressure inclusion assemblage (ky–rt–grt–phg) in the low grossular garnet supports this assumption because although the same assemblage is stable in the orthogneiss the garnet composition predicted for the orthogneiss ($Alm_{60-70}Gr_{30-40}$) does not match the garnet zoning observed in the mica-rich gneiss (Fig. 9).

8. Discussion

In the absence of coesite or another UHP phase proving that the orthogneiss experienced UHP conditions, this study has yielded a number of lines of evidence which suggest that the orthogneiss followed a comparable metamorphic *P–T* path as the eclogite it encloses, with peak pressure at ~26 kbar very close to the quartz–coesite phase boundary. Mineralogical evidence includes the preservation of rare high-pressure phases including high-silica phengite, rutile and kyanite proximal to eclogite blocks, supporting the conclusion that the small rutile, phengite, quartz and kyanite inclusions in garnet are part of a relic high-pressure assemblage which is stable only at very high pressure (~26 kbar) (Fig. 9). Matrix titanite has appreciable amounts of Aluminum (up to 0.23 p.f.u.) which overlaps the range of AlF-substitution observed in the high-pressure titanite in the Luliang Shan eclogites and Dabie Shan orthogneisses (Carswell et al., 2000; Menold et al., submitted for publication).

The phengite in the orthogneiss shows a strong negative correlation between Si and Fe/Mg (Fig. 9), as is generally observed in phengite in eclogite from other UHP localites (Chopin and Ferraris, 2003). This coupled with the prediction that the Ca-poor garnet rims in the orthogneiss grew during increasing temperature and the positive correlation between Ca and Fe/Mg observed in garnet from the mica-rich gneiss support the conclusion from the mafic eclogite that some heating occurred during exhumation (Figs. 6–9). Proyer (2003) using the NKFMASH system with a Dabie Shan orthogneiss predicted that dehydration of phengite during heating and decompression will produce more Fe-rich garnet and Al-rich mica, as is also observed in this study.

Typically, maximum X_{Ca} values in garnet are assumed to represent the pressure maximum (e.g. Carswell et al., 2000, 1997). As this study has shown, this assumption does not hold in all cases and is bulk composition dependent. As orthogneiss garnets commonly have fewer inclusions than their counterparts in intermediate or mafic bulk compositions, caution should be used when using grossular content as a proxy for pressure.

P–T pseudosections provide an additional tool to constrain conditions of metamorphism in samples not suited to thermobarometry. While there are limitations to the method, the pseudosections in this study support and confirm that the petrologic observations and chemical zoning are consistent with the interpretation that the orthogneiss followed a similar clockwise *P–T* path to the eclogite it hosts and that the two lithologies were in contact prior to UHP metamorphism in the North Qaidam. Major element exchange resulting in the bimodal gneiss compositions took place prior to UHP metamorphism. Given the extent of retrograde metamorphism so often observed in felsic rocks hosting mafic and ultramafic UHP rocks, this approach allows the evaluation of the metamorphic *P–T* history of all parts of a UHP terrane independently and the confirmation of high pressure when coesite is absent.

Acknowledgments

We are grateful to C. Mattinson, an anonymous reviewer and S.G. Song (Guest Editor) for critical and constructive review of the manuscript. We thank X.-D. Peng for assistance in the field and F. Kyte for assistance with the electron microprobe. This research was conducted at the University of California, Los Angeles and the University of Innsbruck, Austria. The work was supported by the US National Science Foundation (NSF-EAR-0337191).

References

Barker, F., 1979. Trondjemite: definition, environment and hypothesis of origin. In: Barker, F. (Ed.), Trondjemites, Dacites and Related Rocks. Developments in Petrology, vol. 6. United States Geological Survey, Denver, pp. 1–11.

Biino, G.G., Compagnoni, R., 1992. Very-high pressure metamorphism of the Brossaco coronite metagranite, southern Dora Maira Massif, Western Alps. Swiss Bulletin of Mineralogy and Petrology 72, 347–363.

Carswell, D.A., O'Brien, P.J., Wilson, R.N., Zhai, M., 1997. Thermobarometry of phengite-bearing eclogites in the Dabie Mountains of central China. Journal of Metamorphic Geology 15, 239–252.

Carswell, D.A., Wilson, R.N., Zhai, M., 2000. Metamorphic evolution, mineral chemistry and thermobarometry of schists and orthogneisses hosting ultrahigh pressure eclogites in the Dabieshan of central China. Lithos 52, 121–155.

Chopin, C., Ferraris, G., 2003. Mineral chemistry and mineral reactions in UHPM rocks. EMU Notes in Mineralogy 5, 191–227.

Chopin, C., Henry, C., Michard, A., 1991. Geology and petrology of the coesite-bearing terrain, Dora-Maira Massif, Western Alps. European Journal of Mineralogy 3, 263–291.

Coleman, R.G., Wang, X., 1995. Ultrahigh Pressure Metamorphism. Cambridge Topics in Petrology. Cambridge University Press, UK. p. 528.

Connolly, J.A.D., 1990. Multivariable phase diagrams: an algorithm based on generalized thermodynamics. American Journal of Science 290, 666–718.

Connolly, J.A.D., Kerrick, D.M., 2002. Metamorphic controls on seismic velocity of subducted oceanic crust at 100–250 km depth. Earth and Planetary Science Letters 204, 61–74.

Droop, G.T.R., 1987. A general equation for estimating Fe^{3+} concentrations in ferromagnesian silicates and oxides from microprobe analyses, using stoichiometric criteria. Mineralogical Magazine 51, 431–435.

Enami, M., Suzuki, K., Liou, J.G., Bird, D.K., 1993. Al–Fe^{3+} and F–OH substitutions in titanite and constraints on their *P–T* dependence. European Journal of Mineralogy 5, 219–231.

Ernst, W.G., Liou, J.G., 1995. Contrasting plate-tectonic styles of the Qinling–Dabie–Sulu and Franciscan metamorphic belts. Geology 23, 353–356.

Green, T.H., Hellman, P.L., 1982. Fe–Mg partitioning between coexisting garnet and phengite at high pressures, and comments on a garnet–phengite geothermometer. Lithos 15, 253–266.

Harley, S.L., Carswell, D.A., 1995. Ultradeep crustal metamorphism: a prospective view. Journal of Geophysical Research 100 (B5), 8367–8380.

Holland, T.J.B., 1980. The reaction albite = jadeite + quartz determined experimentally in the range 600–1200 °C. American Mineralogist 65, 129–134.

Holland, T.J.B., Powell, R., 1998. An internally consistent thermodynamic data set with uncertainties and correlations: the system Na_2O–K_2O–CaO–MgO–MnO–FeO–Fe_2O_3–Al_2O_3–SiO_2–TiO_2–C–H_2–O_2. Journal of Metamorphic Geology 8, 89–124.

Jolivet, M., Brunel, M., Seward, D., Xu, Z., Yang, J., Roger, F., et al., 2001. Mesozoic and Cenozoic tectonics of the northern edge of the Tibetan plateau: fission-track constraints. Tectonophysics 343, 111–134.

Kretz, R., 1983. Symbols for rock-forming minerals. American Mineralogist 68, 277–279.

Le Goff, E., Bellevre, M., 1990. Geothermobarometry in albite-garnet orthogneisses: a case study from the Gran Paradiso nappe (Western Alps). Lithos 25, 261–280.

Lenze, A., Stöckhart, B., 2007. Microfabrics of UHP metamorphic granites in the Dora Maira Massif, western Alps – no evidence of deformation at great depth. Journal of Metamorphic Geology 25, 461–475.

Liu, F., Liou, J.G., Xue, H., 2006. Identification of UHP and non-UHP orthogneisses in the Sulu UHP terrane, Eastern China: evidence from SHRIMP U–Pb dating of mineral inclusion-bearing zircons. International Geology Review 48, 1067–1086.

Massonne, H.J., Chopin, C., 1989. *P–T* history of the Gran Paradiso (western Alps) metagranites based on phengite geobarometry. In: Daly, J.S., Cliff, R.A., Yardley, B.W.D. (Eds.), Evolution of Metamorphic Belts. Geological Society (London) Special Publication, vol. 43, pp. 545–549.

Mattinson, C.G., Menold, C.A., Zhang, J.X., Bird, D.K., 2007. High- and ultrahigh pressure metamorphism in the North Qaidam and South Altyn Terranes, Western China. International Geology Review 49, 969–995.

Menold, C.A., Manning, C.E., Yin, A., Chen, X.-H., Wang, X.-F., submitted for publication. Metamorphic evolution, mineral chemistry and thermobarometry of ultrahigh pressure eclogites from the North Qaidam metamorphic belt, Western China. Journal of Metamorphic Geology.

Mirwald, P.W., Massonne, H.J., 1980. The low-high quartz and quartz–coesite transition to 40 kbar between 600 °C and 1600 °C and some reconnaissance data on the effect of $NaAlO_2$ component on the low quartz–coesite transition. Journal of Geophysical Research 85, 6983–6990.

Newton, R.C., Charlu, T.V., Kleppa, O.J., 1980. Thermochemistry of the high structural state plagioclases. Geochimica et Cosmochimica Acta 44, 933–941.

Oberhänsli, R., Hunziker, J.C., Martinotti, G., Stern, W.B., 1985. Geochemistry, geochronology and petrology of Monte Mucrone: an example of eo-Alpine eclogitization of Permian granitoids in the Sesia–Lanzo zone, Western Alps, Italy. Chemical Geology 52, 165–184.

Powell, R., 1985. Regression diagnostics and robust regression in geothermometer/geobarometer calibration: the garnet-clinopyroxene geothermometer revisited. Journal of Metamorphic Geology 3, 231–243.

Proyer, A., 2003. The preservation of high-pressure rocks during exhumation: metagranites and metapelites. Lithos 70, 183–194.

Qinghai BGMR (Bureau of Geology, Mineral Resources), 1991. Regional Geology of Qinghai Province. Geological Publishing House, Beijing, China (in Chinese with English abstract).

Rowley, D.B., Xue, F., Tucker, R.D., Peng, Z.X., Baker, J., Davis, A., 1997. Ages of ultrahigh pressure and protolith orthogneiss from the eastern Dabie Shan: U/Pb zircon geochronology. Earth and Space Science Letters 151, 191–203.

Song, S.G., Yang, J.S., Xu, Z.Q., Liou, J.G., Shi, R.D., 2003a. Metamorphic evolution of the coesite-bearing ultrahigh-pressure terrane in the North Qaidam, Northern Tibet, NW China. Journal of Metamorphic Geology 21, 631–644.

Song, S.G., Yang, J.S., Liou, J.G., Wu, C.L., Shi, R.D., Xu, Z.Q., 2003b. Petrology, geochemistry and isotopic ages of eclogites in the Dulan UHPM terrane, the North Qaidam, NW China. Lithos 70, 195–211.

Song, S.G., Zhang, L.F., Niu, Y., 2004. Ultra-deep origin of garnet peridotite from the North Qaidam ultrahigh-pressure belt, northern Tibetan Plateau, NW China. American Mineralogist 89, 1330–1336.

Song, S.G., Zhang, L.F., Niu, Y., Su, L., Jian, P., Liu, D.Y., 2005a. Geochronology of diamond-bearing zircons from garnet peridotite in the North Qaidam UHPM belt, northern Tibetan Plateau: a record of complex histories from oceanic lithosphere subduction to continental collision. Earth and Planetary Science Letters 234, 99–118.

Song, S.G., Zhang, L.F., Chen, J., Liou, J.G., Niu, Y., 2005b. Sodic amphibole exsolutions in garnet from garnet peridotite, North Qaidam UHPM belt, NW China: implications for ultradeep-origin and hydroxyl defects in mantle garnets. American Mineralogist 90, 814–820.

Song, S.G., Zhang, L.F., Niu, Y., Su, L., Song, B., Liu, D.Y., 2006. Evolution from oceanic subduction to continental collision: a case study of the Northern Tibetan Plateau inferred from geochemical and geochronological data. Journal of Petrology 47, 435–455.

Tabata, H., Yamauchi, K., Maruyama, S., Liou, J.G., 1998. Tracing the extent of a UHP metamorphic terrane: mineral-inclusion study of zircons in gneisses from the Dabie Shan. In: Hacker, B.R., Liou, J.G. (Eds.), When Continents Collide: Geodynamics and Geochemistry of Ultrahigh-Pressure Rocks. Kluwer Academic Publishing, Netherlands, pp. 261–273.

Troitzsch, U., Ellis, D.J., 2002. Thermodynamic properties and stability of AlF-bearing titanite $CaTiOSiO_4$–$CaAlFSiO_4$. Contributions to Mineralogy and Petrology 142, 543–563.

Wallis, S.R., Ishiwatari, A., Hirajima, T., Ye, K., Guo, J., Nakamura, D., Kato, T., Zhai, M., Enami, M., Cong, B., Banno, S., 1997. Occurrence and field relationship of ultrahigh-pressure metagranitoid and coesite eclogite in the Su-Lu terrane, eastern China. Journal of the Geological Society (London) 154, 45–54.

Yang, J.S., Xu, Z.Q., Song, S.G., 2000. Discovery of eclogite in Dulan, Qinghai Province and its significance for studying the HP–UHP metamorphic belt along the central orogenic belt of China. Acta Geologica Sinica 74, 156–168 (in Chinese with English abstract).

Yang, J.S., Xu, Z.Q., Zhang, J.X., Chu, J.Y., Zhang, R.Y., Liou, J.G., 2001a. Tectonic significance of early Paleozoic high-pressure rocks in Altun–Qaidam–Qilian Mountains, NW China. Geological Society of America Memoir 194, 151–170.

Yang, J.S., Song, S.G., Xu, Z.Q., Liu, F.L., Maryyama, S., Liou, J.G., Zhang, J.X., Wu, C.L., Li, H.B., Shi, R.D., 2001b. Discovery of coesite in the north Qaidam Caledonian ultrahigh–high-pressure (UHP–HP) metamorphic belt on the northeastern Qinghai-Tibet plateau. In: Eleventh Annual VM Goldschmidt Conference, vol. 3088.

Yang, J.S., Xu, Z.Q., Zhang, J.X., Song, S.G., Wu, C.L., Shi, R.D., Li, H.B., Brunel, M., 2002. Early Paleozoic North Qaidam UHP metamorphic belt on the north-eastern Tibetan plateau and a pair subduction model. Terra Nova 14, 397–404.

Ye, K., Cong, B., Ye, D., 2000. The possible subduction of continental material to depths greater than 200 km. Nature 407, 734–736.

Yin, A., Harrison, T.M., 2000. Geologic evolution of the Himalayan–Tibetan orogen. Annual Review of Earth Planetary Sciences 28, 211–280.

Yin, A., Rumelhart, P.E., Butler, R., Cowgill, E., Harrison, T.M., Foster, D.A., Ingersoll, R.V., Zhang, Q., Zhou, X.Q., Wang, X.F., Hanson, A., Raza, A., 2002. Tectonic history of the Altyn Tagh Fault system in northern Tibet inferred from Cenozoic sedimentation. Geological Society of America Bulletin 114, 1257–1295.

Zhang, J.X., Zhang, Z.M., Xu, Z.Q., Yang, J.S., Cui, J.W., 2001. Petrology and geochronology of eclogites from the western segment of the Altyn Tagh, northwestern China. Lithos 56, 187–206.

Zhang, J.X., Yang, J.S., Xu, Z.Q., Meng, F.C., Li, H.B., Shi, R.D., 2002. Evidence for UHP metamorphism of eclogites from the Altun Mountains. Chinese Science Bulletin 47 (9), 751–755.

Zhang, J., Meng, F., Yang, J., 2004. Eclogitic metapelites in the western segment of the north Qaidam Mountains: evidence on "in situ" relationship between eclogite and its country rock. Science in China, Series D 47, 1102–1112.

Zhang, J.X., Yang, J.S., Mattinson, C.G., Xu, Z.Q., Meng, F.C., Shi, R.D., 2005a. Two contrasting eclogite cooling histories, North Qaidam HP/UHP terrane, western China: petrological and isotopic constraints. Lithos 84, 51–76.

Zhang, J.X., Mattinson, C.G., Meng, F.C., Wan, Y.S., 2005b. An early Paleozoic HP/HT granulite-garnet peridotite associations in the south Altyn Tagh, NW China: *P–T* history and U–Pb geochronology. Journal of Metamorphic Geology 23, 491–510.

Zhang, J.X., Meng, F., Yang, J.S., 2005c. A new HP/LT metamorphic terrane in the northern Altyn Tagh, western China. International Geology Review 47, 371–386.